ЖЭТФ, 2014, том 146, вып. 4 (10), стр. 675–684 © 2014

STABILIZING OPTICAL FEEDBACK-INDUCED CHAOS BY SINUSOIDAL MODULATION BEYOND THE RELAXATION FREQUENCY IN SEMICONDUCTOR LASERS

A. H. Bakry, M. Ahmed*

Department of Physics, Faculty of Science, King Abdulaziz University
20803, Jeddah 21589, Saudi Arabia

Received February 13, 2014

We report on stabilizing the chaotic dynamics of semiconductor lasers under optical feedback (OFB) by means of sinusoidal modulation at frequencies far beyond the relaxation frequency of the laser. The laser is assumed to be coupled to a short external cavity, which is characterized by a resonance frequency spacing higher than the relaxation frequency. The study is based on a time delay rate equation model of OFB, which is suitable for treating the regime of strong OFB and considering multiple reflections in the external cavity. We show that the intensity modulation response of the chaotic laser under strong OFB is enhanced over a narrow frequency band near the doubled relaxation frequency due to a photon–photon resonance. Within this high-frequency band, the sinusoidal modulation may convert the chaotic attractor to a limit cycle, and the small-signal modulation suppresses the relative intensity noise (RIN) to a level only 2 dB higher than the RIN level of the solitary laser.

DOI: 10.7868/S0044451014100010

1. INTRODUCTION

In most of its applications, a semiconductor laser is subjected to an amount of external optical feedback (OFB), such as the back reflection by the reflecting surface in the optical disc system or by the fiber facet in the optical fiber links. OFB may stabilize the laser operation, but on the other extreme, it may cause violent instabilities in the form of chaos, depending on the feedback parameters [1]. The chaotic dynamics under OFB is associated with a state of coherence collapse, which is manifested as significant broadening of the laser line shape and enhanced noise levels [2–5]. Experiments show that the noise level is increased by 20 dB or more as a result of OFB [6]. Intensive research activities have been focused on the control of the chaos dynamics and suppression of the associated noise of lasers [7–18]. Superposition of a high-frequency (HF) current is the most popularly used method to suppress the OFB noise. The OFB noise is well suppressed by suitable selections of the frequency and amplitude of the superposed current. It has been established that the frequency window of the sinusoidal modulation for stabilizing the chaotic dynamics is around the relaxation frequency of the laser. Beyond the relation frequency, the intensity modulation (IM) response drops to lower orders and reaches the -3 dB level at the modulation bandwidth. It was shown in [17] that in the vicinity of the relaxation frequency, chaos is converted into period-1 oscillations or period doubling, depending on the modulation depth. The noise level in the low-frequency regime was predicted to be about 8 dB/Hz higher than the quantum noise level of the solitary laser [17]. This noise difference occurs mainly because the regime of the relaxation frequency is characterized by a strong coupling between the emitted photons and the injected carriers and by harmonic distortions of the laser signal [19], which contribute to the increase in relative intensity noise (RIN). It is also worth noting that previous studies on controlling chaos by sinusoidal modulation were concerned with intermediate OFB strengths. However, chaos is also induced by strong OFB [5], and hence extending the previous studies to the regime of strong OFB is necessary.

With the external OFB strength varied, the semiconductor laser exhibits a number of chaos regions. The length of the external cavity controls not only the

*E-mail: mostafa.hafez@science.miniauniv.edu.eg. On leave from Department of Physics, Faculty of Science, Minia University, Egypt.

number and the OFB range of these chaotic regions but also the route to chaos [20, 21]. In semiconductor lasers coupled to a short external cavity, the route to chaos is of the period-doubling type [20, 21]. The oscillation frequency along these chaos regions increases with the increase in the OFB strength; it starts with the relaxation frequency and ends with the resonance frequency separation of the external cavity in the region of strong OFB [20]. Therefore, OFB has been used to increase the modulation bandwidth of semiconductor laser subjected to strong OFB by a short-distant reflector [5, 22, 23]. Recent investigations by the authors have shown that strong OFB suppresses the IM response below the -3 dB level at the modulation frequencies lower than the carrier-photon resonance (relaxation) frequency [24]. This suppression of the IM response is then followed by enhancement of the modulation response over a narrow band of modulation frequencies much higher than the relaxation oscillation. The enhanced modulation response over the millimeter-wave band 54.5–56.5 GHz was reported for a laser diode with an external cavity 0.15 cm in length [24]. This modulation response enhancement was explained as the photon–photon resonance between two spectrally neighbored longitudinal modes at frequencies exceeding the relaxation oscillation [24, 25]. It has been shown that within the frequency band of the enhanced IM response, the sinusoidal modulation releases period-1 oscillations with low signal distortion and suppressed noise levels [26]. These findings motivate the authors to examine the possibility of stabilizing the OFB-induced chaotic dynamics and suppressing the associated noise of the laser by modulation the laser far beyond the relaxation frequency.

In this paper, we investigate the stability of the chaotic dynamics under modulation frequencies within the frequency band of the enhanced IM response and examine the noise suppression effect. The study is based on an improved time-delay rate equation model of semiconductor lasers augmented by a sinusoidal current signal as well as intrinsic noise sources. The multiple reflections of laser radiation in the external cavity are taken into account. The present model is applicable to laser cavities supporting single-mode oscillations. Examples include distributed feedback (DFB) lasers, vertical-cavity surface-emitting lasers (VCSELs) with selective oxidation for current and photon confinement [27], and Fabry–Perot (FP) lasers with well-controlled transverse structures, in which mode competition induces the side-mode suppression ratio higher than 20 dB [28]. The model can also be generalized to treat OFB in semiconductor lasers with multimode oscillations [29]. The noise properties of the modulated signal are determined in terms of RIN and its average value, LF-RIN, in the low-frequency regime. The laser dynamics are analyzed and classified based on the waveform of the laser and its fast Fourier transform (FFT) as well as on the phase portrait of the photon number versus the injected carrier number. We apply the present study to a 1.55 μm InGaAsP laser coupled to a short external cavity with a relaxation frequency of 4.5 GHz. We show that the modulation response of the chaotic laser due to strong OFB is enhanced over a narrow frequency band beyond 9 GHz, which is twice the relaxation frequency. Within this high-frequency band, the sinusoidal modulation turns out to attract the chaotic attractor to a stable state with periodic-1 oscillations, and the small-signal modulation could suppress RIN to that of a solitary laser.

In the next section, the time-delay rate equation model of laser dynamics and noise under OFB is introduced. Section 3 introduces the procedures of numerical calculations. Section 4 presents the results of modulation dynamics and noise under OFB. The conclusions of the present work appear in the last section.

2. THEORETICAL MODEL

The proposed laser structure is composed of a laser diode oscillating in a single mode and coupled to an external cavity formed by placing an external reflector of power reflectivity R_{ex} at a distance L_{ex} from the front facet of the laser. The laser has a length L_D, a refractive index n_D and power reflectivities R_f and R_b at the front and back facets. OFB is treated as the time delay of laser light of the electric field due to round trips in the external cavity. The round-trip time, or time delay, is $\tau = 2n_{ex}L_{ex}/c$, where n_{ex} is the refractive index of the external cavity. The present time-delay model of OFB is illustrated by the scheme in Fig. 1. At a time t,

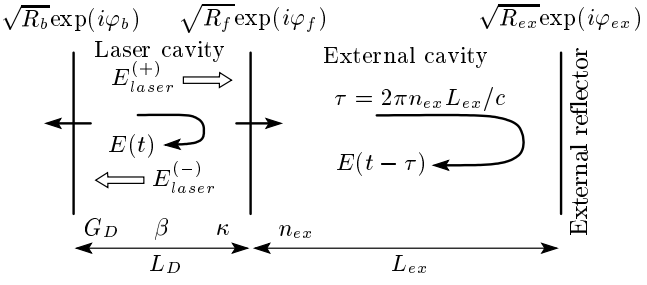

Fig. 1. Scheme of the proposed model of semiconductor lasers under OFB

the boundary conditions of the laser at the back facet ($z = 0$) and the front facet ($z = L_D$) are then modified to [30]

$$E^{(+)}_{laser}(0,t) = \sqrt{R_b}\,\exp\{-i\varphi_b\}\,E^{(-)}_{laser}(0,t), \quad (1)$$

$$E^{(+)}_{laser}(L_D,t) = \\ = \sqrt{R_f}\,\exp\{-i\varphi_f\}\,U(t-\tau)E^{(-)}_{laser}(L_D,t). \quad (2)$$

Here, $E^{(+)}_{laser}$ and $E^{(-)}_{laser}$ are the forward and backward propagating components of the electric field inside the laser cavity, and $U(t-\tau)$ is the time-delay function, which accounts for the OFB due to multiple round trips (reflections) in the external cavity and is given by [30]

$$U(t-\tau) = |U|\exp\{-j\varphi\} = \\ = 1 - \sum_{p=1}(K_{ex})^p \left(\frac{R_f}{1-R_f}\right)^{p-1} \times \\ \times \exp\{-ip\omega\tau\}\frac{S(t-p\tau)}{S(t)}\,\frac{\exp\{i\theta(t-p\tau)\}}{\exp\{i\theta(t)\}}, \quad (3)$$

where $S(t)$ and $\theta(t)$ are respectively the photon number and optical phase of the field, $S(t-\tau)$ and $\theta(t-\tau)$ are the corresponding time-delay values, and p is an index for the round trips. The exponent $\omega\tau$, where ω is the angular frequency of the laser emission, represents the OFB phase due to delay of the optical field in one round trip. The OFB strength is measured by the coefficient

$$K_{ex} = (1-R_f)\sqrt{\eta\frac{R_{ex}}{R_f}}, \quad (4)$$

with η being the coupling efficiency of light injected into the laser cavity. In equations (1) and (2), ϕ_f and ϕ_b are the optical phases at the front and back facets. Therefore, the exponentional gain per pass is modified to

$$1 = \sqrt{R_f R_b}\,|U(t-\tau)|\exp\{(g-\kappa)L_D\} \times \\ \times \exp\{-i(2\beta L_D + \varphi_f + \varphi_b + \varphi)\}, \quad (5)$$

where g, κ, and β are the gain per unit length, internal loss, and the propagation constant in the laser cavity. The threshold gain and phase conditions of the laser are then modified to

$$G_{th} = G_{thD} - \frac{c}{n_D L_D}\ln|U(t-\tau)|, \quad (6)$$

$$2\beta L_D + \varphi_f + \varphi_b + \varphi = 2s\pi, \quad (7)$$

where s is an integer and

$$G_{thD} = \frac{c}{n_D}\left[\kappa + \frac{1}{2L_D}\ln\frac{1}{R_f R_b}\right] \quad (8)$$

is the threshold gain (per sec) in the solitary laser.

The modulation characteristics and noise of the semiconductor laser under both external OFB and IM are then described by the following time-delay rate equations for the carrier number $N(t)$, the photon number $S(t)$, and the optical phase $\theta(t)$ [30]:

$$\frac{dN}{dt} = \frac{1}{e}I(t) - \frac{N}{\tau_s} - \frac{a\xi}{V}(N-N_g)S + F_N(t), \quad (9)$$

$$\frac{dS}{dt} = \left[\frac{a\xi}{V}(N-N_g) - B_c(N-N_s)S - \right. \\ \left. - G_{thD} + \frac{1}{n_D L_D}\ln|U(t-\tau)|\right]S + \\ + C\frac{N}{\tau_s} + F_S(t), \quad (10)$$

$$\frac{d\theta}{dt} = \frac{1}{2\pi}\Delta\nu = \frac{1}{2}\left(\alpha\frac{a\xi}{V}(N-\overline{N}) - \frac{c}{n_D L_D}\varphi\right) + \\ + F_\theta(t), \quad (11)$$

where $\Delta\nu(t)$ is the shift of the lasing frequency (frequency chirp) associated with the intensity modulation. The laser parameters in Eqs. (9)–(11) are defined as follows: a is the differential gain coefficient, G_{thD} is the threshold gain of the solitary laser, ξ is the field confinement factor, V is the volume of the laser cavity whose length is L_D and refractive index is n_D, N_g is the electron density at transparency, N_s is an electron number characterizing the nonlinear gain suppression whose coefficient is B_c, and τ_s is the electron lifetime due to the spontaneous emission whose fraction into the stimulated emission is C. In Eq. (11), $\overline{N}$ is the time average value of $N(t)$ in the solitary laser. The injection current is composed of a bias component I_b and a modulation component. The latter is characterized by the modulation current I_m and the frequency f_m:

$$I(t) = I_b + I_m\sin(2\pi f_m t). \quad (12)$$

Both I_b and I_m define the modulation depth $m = I_m/I_b$.

The last terms $F_N(t)$, $F_S(t)$, and $F_\theta(t)$ in rate equations (9)–(11) are Langevin noise sources with zero means, and are added to the equations to account for intrinsic fluctuations of the laser [31]. These noise sources are assumed to have Gaussian probability distributions and to be δ-correlated processes [31]. The noise content of the fluctuations in the photon number $S(t)$ around its time average value $\overline{S}$ is determined in terms of RIN over a finite time T as [31]

$$RIN = \frac{1}{\overline{S}^2} \times \times \left\{ \frac{1}{T} \left| \int_0^T \left(S(t) - \overline{S}\right) \exp\left\{-i2\pi f \tau\right\} d\tau \right|^2 \right\}, \quad (13)$$

where f is the Fourier frequency. According to the above equation, the RIN spectrum includes not only the noise but also the signal power spectral density.

3. NUMERICAL CALCULATIONS

Rate equations (9)–(11) are solved by the 4th-order Runge–Kutta method using the time integration step $\Delta t = 5$ ps. We adapt the length of the external cavity to be $n_{ex}L_{ex} = 1.5$ cm, which corresponds to the external-cavity resonance frequency spacing $f_{ex} = 10$ GHz. We count five roundtrips ($p = 1 \to 5$ in Eq. (3)), each of the duration $\tau = 1/f_{ex} = 0.1$ ns, in the calculations. The integration is taken over a long period of time $T = 6$ μs, with all terms $S(t - p\tau)$ and $\theta(t - p\tau)$ regarded as time delayed values. Both the modulation response and the spectrum of RIN are calculated over the time period between 4 and 6 μs, during which the state of the laser operation does not change. At each integration step, the noise sources $F_N(t)$, $F_S(t)$, and $F_\theta(t)$ are generated by applying the technique in [31] using a set of uniformly distributed random numbers generated by the computer. In Table, we list the values of the laser parameters used in the calculations, which correspond to 1.55 μm semiconductor lasers. In these narrow bandgap lasers, the spontaneous emission lifetime is given in terms of the nonradiative recombination rates due to crystal defects A_{nr} and Auger processes C_{AUG}, and the radiative recombination rate B_r as

$$\tau_s = \left[A_{nr} + B_r(N/V) + C_{AUG}(N/V)^2\right]^{-1}. \quad (14)$$

We computed RIN from the calculated values of $S(t_i)$ by using the FFT to calculate the discrete version of Eq. (13) as

$$RIN \equiv \frac{1}{\overline{S}^2} \frac{\Delta t^2}{T} \left[\mathrm{FFT}\left(S(t_i) - \overline{S}\right)\right]^2. \quad (15)$$

4. RESULTS AND DISCUSSION

The laser is assumed to be biased far above the threshold, $I_b = 3I_{th}$, with I_{thD} being the threshold current of the solitary laser. The corresponding relaxation frequency f_r is determined approximately from the small-signal approach as [32]

$$f_r \approx \frac{1}{2\pi} \times \times \sqrt{\frac{a\xi}{V}\left[\frac{a\xi\tau_e}{eV}(I_b - I_g) + B\frac{I_b - I_{thD}}{eG_{thD}}\right]\frac{I_b - I_{thD}}{eG_{thD}}}, \quad (16)$$

where I_g is the transparency current and $B = B_c(N_{th} - N_s)$. The calculated value is $f_r \approx 4.5$ GHz, which means that the frequency ratio $f_{ex}/f_r = 2.22$. Therefore, the present laser dynamics under OFB are characterized by a period-doubling route-to-chaos, as illustrated in Refs. [20, 21]. The frequency of possible oscillations under strong OFB increases with an increase in the OFB strength; it starts with the relaxation oscillation f_r in the route to chaos in the weak OFB regime and approaches the external-cavity resonance frequency $f_{ex} = 10$ GHz in the regime of strong OFB [20].

4.1. Chaotic dynamics and noise in a solitary laser

4.1.1. Temporal characteristics of the chaotic state

In this section, we characterize the chaotic dynamics of the laser induced by OFB. These characteristics include the temporal trajectories of both the intensity and frequency chirp of the laser as well as the phase portrait. These characteristics are plotted in Fig. 2 for three chaotic states induced when $K_{ex} = 0.16$ (intermediate OFB), 0.27 (rather strong OFB), and 0.56 (strong OFB). The injection current is $I_b = 3I_{thD}$. Figures 2*a–c* plot the temporal trajectories of the emitted photon number $S(t)$, Figs. 2*d–f* plot the temporal variations of the associated frequency chirp $\Delta\nu(t)$, and Figs. 2*g–i* plot the phase portraits of the photon number $S(t)$ versus the carrier number $N(t)$. In these figures, both $S(t)$ and $N(t)$ are normalized by the corresponding time-averaged values $\overline{S}$ and $\overline{N}$. In these relevant three cases of chaos, Figs. 2*a–f* show that both $S(t)$ and $\Delta\nu(t)$ are characterized by irregular variations as time progress. The maximum induced chirps are 144, 149, and 182 GHz for the respective values $K_{ex} = 0.16$, 0.27, and 0.56. These temporal irregularities of the chaos states are manifested as chaotic attractors in the phase portraits in Figs. 2*g–i*.

Table. List of the parameters of 1.55 μm InGaAsP lasers and their typical values used in the calculations

Parameter	Value
Emission wavelength λ	1550 nm
Tangential gain coefficient a	$7.96 \cdot 10^{-12}$ m$^3 \cdot$ s^{-1}
Field confinement factor in the active layer ξ	0.2
Volume of the active region V	150 μm^3
Length of the active region L_D	300 μm
Refractive index of the active region n_D	3.53
Electron number at transparency N_g	$1.32 \cdot 10^8$
Electron number characterizing gain suppression N_s	$1.012 \cdot 10^8$
Coefficient characterizing gain suppression B_c	$3.18 \cdot 10^{-4}$ s^{-1}
Linewidth enhancement factor α	5
Front facet reflectivity R_f	0.2
Back facet reflectivity R_b	0.9
Threshold gain level G_{thD}	$2.44 \cdot 10^{11}$ s^{-1}
Threshold current I_{thD}	8 mA
Nonradiative recombination coefficient A_{nr}	10^8 s^{-1}
Radiative recombination coefficient B_r	$3.6 \cdot 10^{-16}$ m^3/s
Auger recombination coefficient C_{AUG}	$0.3 \cdot 10^{-41}$ cm^6/s

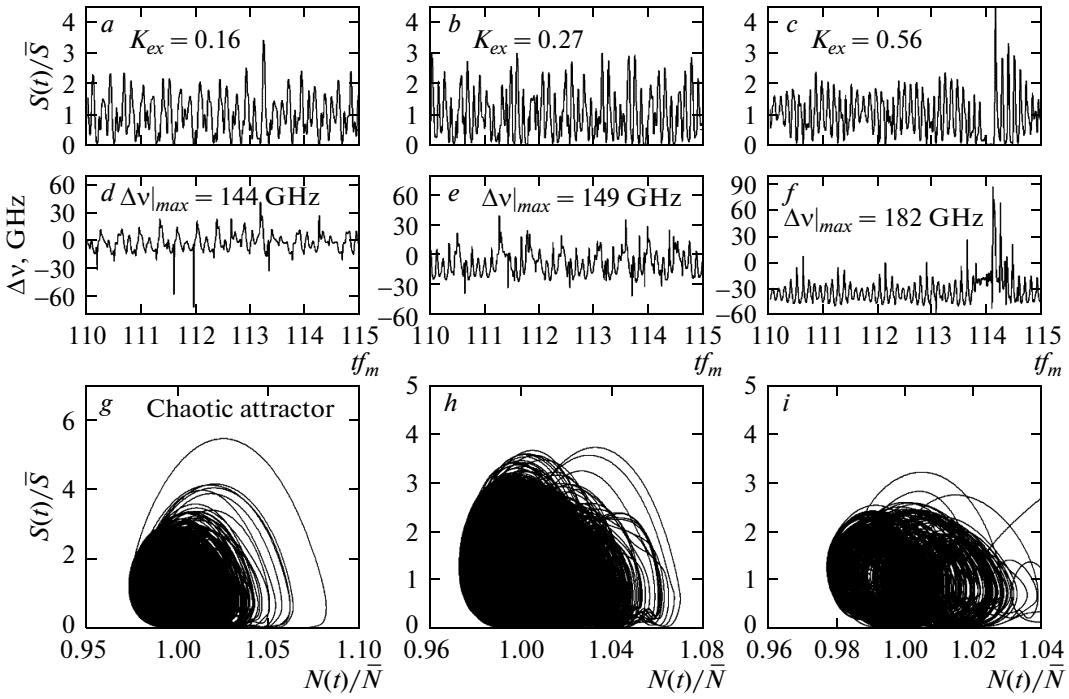

Fig. 2. Characteristics of the chaotic dynamics: a–c temporal trajectories of $S(t)$, d–f temporal trajectories of $\Delta\nu(t)$, and g–i ($S(t)$ versus $N(t)$) phase portraits, with $K_{ex} = 0.16$, 0.27, and 0.56

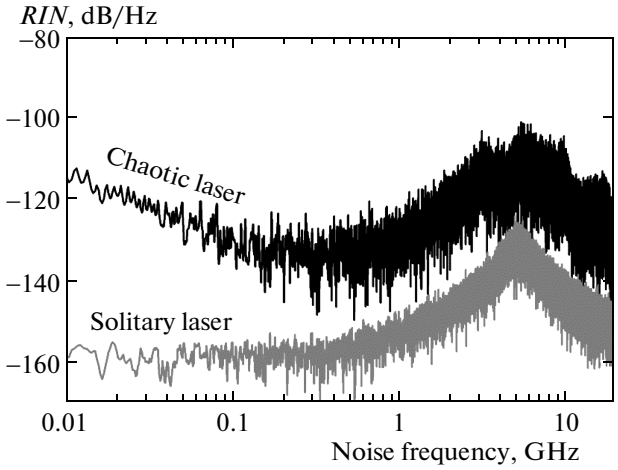

Fig. 3. Frequency spectrum of RIN of the solitary laser and the chaotic laser under OFB with $K_{ex} = 0.16$ when $I_b = 3I_{thD}$

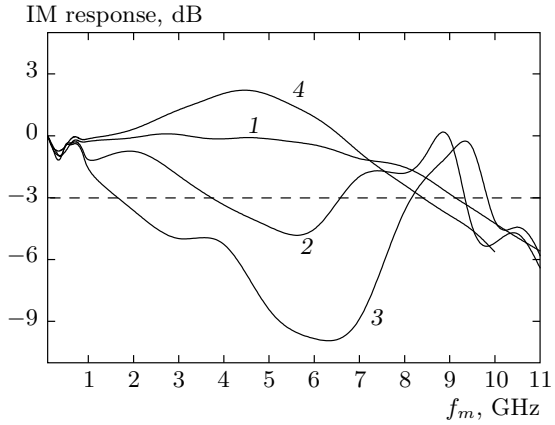

Fig. 4. IM responses of the chaotic laser with $K_{ex} = 0.16$ (*1*), 0.27 (*2*), and 0.56 (*3*) and the nonchaotic solitary laser (*4*) when $m = 0.5$

4.1.2. Intensity noise of a nonmodulated laser

The spectral properties of RIN of the chaotic nonmodulated laser are described in Fig. 3. The figure plots an example of the frequency spectrum of RIN and compares it with the RIN spectrum of the solitary laser. In this case, $K_{ex} = 0.23$ and $I_b = 3I_{thD}$. The RIN spectrum of the solitary laser exhibits a peak around the relaxation frequency f_r. The relaxation oscillations are manifestation of the electron–photon resonance. Below the regime of f_r, RIN is flat (white noise), and the low-frequency RIN, which determines the signal-to-noise ratio, is LF-RIN = −160 dB/Hz. As the figure shows, the chaotic RIN spectrum is higher than that of the solitary laser; the high-frequency regime is almost three orders of magnitude higher, while the low-frequency regime is almost six orders of magnitude higher. The level of the low-frequency noise is LF-RIN = −112 dB/Hz. Another indication of the chaotic dynamics is that the resonance peak is hardly indicated in the RIN spectrum. These effects along with the large values of the frequency chirp are manifestations of a state of coherence collapse in the lasing action. These characteristics agree with those reported in [4] and [5].

4.2. Dynamics of the chaotic laser under sinusoidal modulation

Examination of the IM response spectrum of the chaotic laser due to OFB helps explore the modulation frequencies at which the chaotic state could be converted into stable operation. The FFT is used to calculate the IM response as

$$\text{IM repsonse} = a_1(f_m)/a_1(f_m \to 0), \qquad (17)$$

where $a_1(f_m)$ is the amplitude of the fundamental harmonic of the FFT spectrum of the laser intensity at the modulation frequency f_m. In Fig. 4, we plot the calculated IM responses of the laser under the three relevant OFB strengths $K_{ex} = 0.16$, 0.27, and 0.56, and compare them with the IM response of the solitary laser. The modulation depth is set to be $m = 0.5$. The figure shows that the IM response of the solitary laser reveals a peak due to the photon-carrier resonance when the modulation frequency f_m is close to the relaxation frequency $f_r = 4.5$ GHz. The calculated value of the 3 dB-modulation bandwidth is $f_{3\,dB} = 7.2$ GHz.

In the case of the chaotic dynamics under the intermediate OFB with $K_{ex} = 0.16$, the IM response becomes almost flat, and the modulation bandwidth $f_{3\,dB}$ increases to 9.1 GHz. This increase in $f_{3\,dB}$ could be due to the increase in the laser intensity [32]; $\overline{S}$ increases from $3.9 \cdot 10^5$ in the solitary laser to $4 \cdot 10^5$ in the chaotic laser. As the OFB strength increases to $K_{ex} = 0.27$, the IM response of the chaotic laser exhibits the interesting feature that it drops under the −3 dB level at the modulation frequency of 3.7 GHz, which is much lower than $f_{3\,dB}$ of the solitary laser. The further increase in f_m results in enhancement of the IM response over the narrow frequency band 6.6–9.3 GHz, which then extends beyond $f_{3\,dB}$ of the solitary laser. This IM response enhancement can be interpreted as a photon–photon resonance between the

modulating field and an oscillating mode of the external cavity [24,25]. The further increase in K_{ex} to 0.56 results in 1) more reduction in the photon–carrier resonance frequency, with the value of the normal $f_{3\,dB}$ reducing to 1.6 GHz, and 2) a shift of the photon–photon resonance frequency band to higher frequencies (8.2–9.8 GHz). This shift of the frequency band of the enhanced modulation response with the increase in the OFB strength is consistent with the prediction in [24] that the photon–photon resonance frequency increases toward the external-cavity resonance frequency f_{ex} with the increase in K_{ex}.

Investigation of the dynamics of the chaotic laser within the frequency band of the enhanced IM response indicated that the laser exhibits period-1 signals over certain frequencies. Examples of these large-signal regular dynamics are given in Figs. 5 and 6 for the cases where $K_{ex} = 0.27$ and 0.56. The modulation frequency is then $f_m = 9$ GHz, which is twice the relaxation frequency f_r. Figures 5*a* and 6*a* plot the temporal trajectories of the emitted photon number $S(t)$, and show that the modulated signal is of the period-1 type with a high degree of uniformity. The corresponding periodic variation in the frequency chirp $\Delta\nu(t)$ is shown in Figs. 5*b* and 6*b*, which indicate not only the periodic and uniform variation with time but also a remarkable reduction in the maximum frequency chirp. The maximum chirp reduces from $\Delta\nu(t)|_{max} = 144$ and 149 GHz of the chaotic states with $K_{ex} = 0.27$ and 0.56 to the much smaller respective values 31 and 27 GHz under the high-frequency modulation. The high degree of regularity of the modulated laser signal is indicated by the phase portraits in Figs. 5*c* and 6*c*, which show that the sinusoidal modulation converts the chaotic attractors to a single attractor of stable operation. The attractors are not circular because the emitted signals are not sinusoidal in this case of rather deep modulation, $m = 0.5$ [17]. The periodicity and the distortion in the simulated signals are examined by using the FFT power spectrum plotted in Figs. 5*d* and 6*d*. The signal periodicity is manifested in the figures as a sharp and strong peak at the modulation frequency f_m as well as weaker peaks at the higher harmonics. These higher harmonics correspond to 2nd-order harmonic distortion (2HD) and 3rd-order harmonic distortion (3HD) of the signal. These higher-order harmonic distortions are calculated as

$$2\text{HD} = 10\log(a_2/a_1), \quad 3\text{HD} = 10\log(a_3/a_1), \quad (18)$$

where a_2 and a_3 are the amplitudes at the 2nd and 3rd harmonics. The calculated values of 2HD and 3HD are less than -3 dB; they are 2HD $= -4.4$ and 3HD $= -8.4$ dB for $K_{ex} = 0.27$, and 2HD $= -5.1$ and 3HD $= -9.8$ dB for $K_{ex} = 0.27$.

It is worth noting that the large varations of the photon number in both the nonmodulated chaotic laser (Fig. 2) and the modulated chaotic laser (Figs. 5 and 6) with respect to the average value may induce rather large temporal variations in the laser temperature. This temperature variation may induce variations in the laser characteristics and affect the device performance. But in this paper, the frequency regime of interest ranges between 4 and 10 GHz, whereas the thermal frequency response of the laser is below 10 MHz [33, 34]. Therefore, the thermal dynamics is beyond the scope of the present study. Nevertheless, studying the thermal dynamics under the rich dynamics of the semiconductor laser under OFB is needed for further understanding of the laser physics and could be the subject of future research.

4.3. Suppression of the chaotic RIN by small-signal modulation with $f_m \gg f_r$

In the techniques of superposing a high-frequency current, the modulating signal is small and the modulation frequency is in the vicinity of the relaxation frequency f_r of the laser, i. e., in the regime of the photon-carrier resonance. In this subsection, we newly show that small-signal modulation can also be applied to suppress RIN at modulation frequencies much higher than f_r; namely, within the frequency band of the enhanced IM response due to the photon–photon resonance. Figure 7 plots the frequency spectrum of RIN of the chaotic laser when the OFB strength is $K_{ex} = 0.16$, 0.27, and 0.56 under the application of small-signal modulation ($m = 0.1$) with the modulation frequencies f_m much higher than f_r. Figure 7*a* corresponds to the case of the chaotic laser with $K_{ex} = 0.16$ under modulation with $f_m = 8.6$ GHz. The figure has an enhanced peak at the modulation frequency f_m and a much weaker peak at the 2nd harmonic. In contrast to the RIN spectrum of the nonmodulated chaotic laser in Fig. 3*a*, the RIN is flat (white noise) in the low-frequency regime. This feature is similar to the noise spectrum of the nonmodulated solitary laser in Fig. 3*a*. Moreover, the level of the low-frequency RIN is close to that of the solitary laser, LF-RIN $= -158$ dB/Hz, i. e., the noise is just 2 dB higher than that of the solitary laser. This value is smaller than the RIN difference of 8 dB obtained when the chaotic laser is modulated close

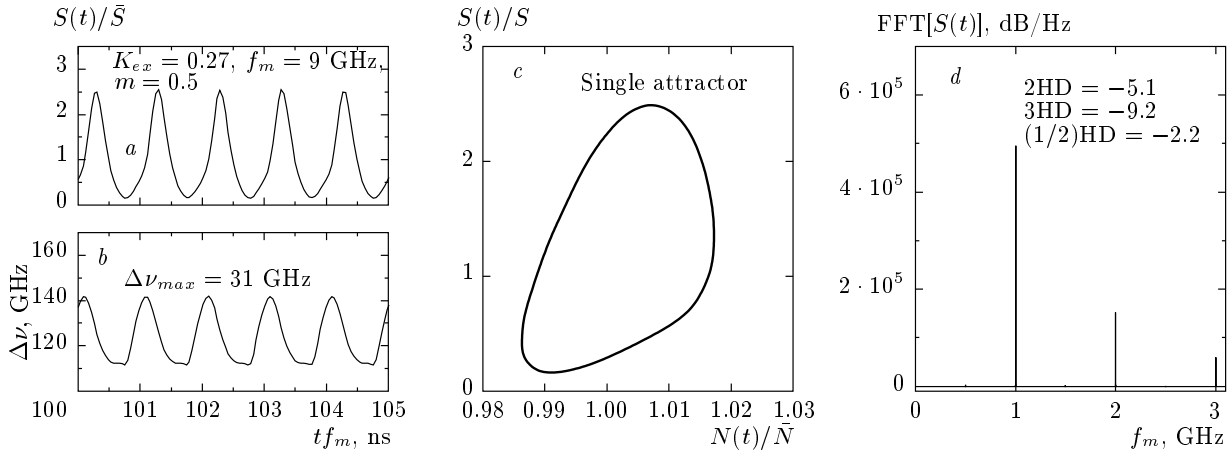

Fig. 5. Characteristics of modulated signal of the chaotic laser with $K_{ex} = 0.27$ and $m = 0.5$: *a*) temporal trajectory of $S(t)$, *b*) temporal trajectory of $\Delta\nu(t)$, *c*) ($S(t)$ versus $N(t)$) phase portraits, and *d*) frequency FFT spectrum of $S(t)$

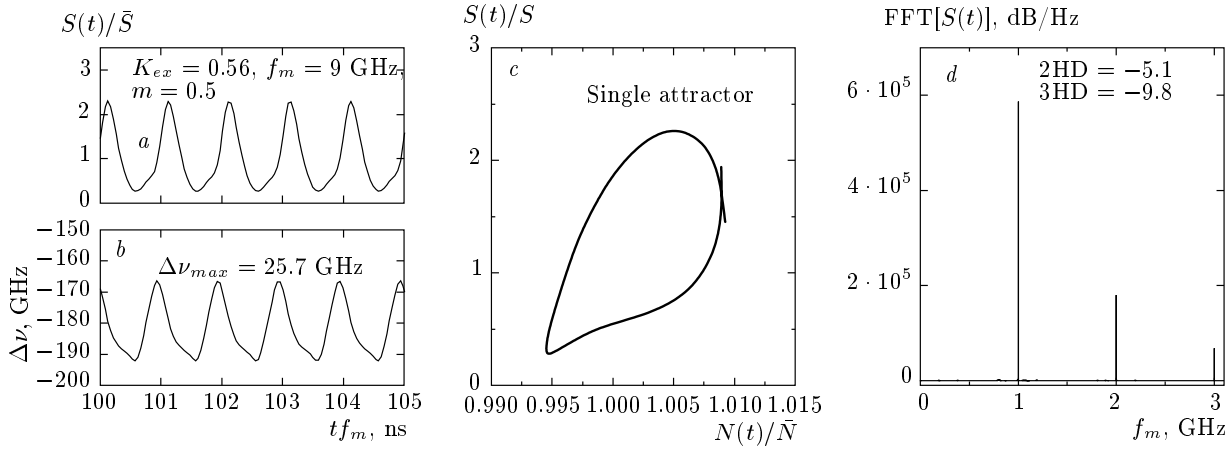

Fig. 6. Characteristics of modulated signal of the chaotic laser with $K_{ex} = 0.56$ and $m = 0.5$: *a*) temporal trajectory of $S(t)$, *b*) temporal trajectory of $\Delta\nu(t)$, *c*) ($S(t)$ versus $N(t)$) phase portraits, and *d*) frequency FFT spectrum of $S(t)$

to the f_r [17]. Similar results are shown in Fig. 7*b* for the chaotic laser with $K_{ex} = 0.27$ when modulated at $f_m = 9.1$ GHz and in Fig. 7*c* for the chaotic laser with $K_{ex} = 0.56$ when modulated at $f_m = 9.6$ GHz.

5. CONCLUSIONS

We investigated the stability and noise suppression of semiconductor lasers coupled to a short external cavity by means of sinusoidal modulation at frequencies exceeding twice the relaxation frequency of the laser. These frequencies lie in a narrow band of the modulation frequencies within which the IM response is enhanced due to a photon–photon resonance. The performance of this high-frequency modulation technique is assessed in terms of the waveform and distortion of the modulated signal and the small-signal frequency spectrum of RIN.

The obtained results show that under intermediate and strong OFB, the laser may exhibit chaotic dynamics characterized by chaotic attractors. Under intermediate OFB, the IM response of the chaotic laser is flat, does not reveal the carrier-photon resonance peak of the solitary laser, and has a higher modulation bandwidth $f_{3\,dB} = 9.1$ GHz. Under stronger OFB, the IM response drops below the -3 dB level at the modulation frequencies lower than the conventional bandwidth, and is enhanced over a narrow frequency band. This interesting frequency band extends beyond $2f_r$ and is close to the resonance frequency of the external cavity. Within this characteristic high frequency band, the sinusoidal modulation happens to stabilize

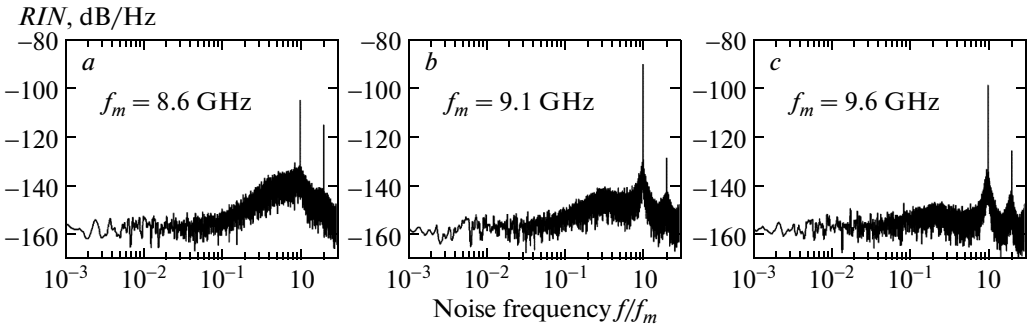

Fig. 7. Frequency spectra of RIN of the chaotic laser under sinusoidal modulation with $m = 0.1$, for $K_{ex} = 0.16$ (a), 0.27 (b), and 0.56 (c)

the chaotic dynamics; it converts the chaotic attractor to a periodic single state. The stabilized dynamics are characterized by periodic and uniform output signals with harmonic distortions as low as 2HD ≈ -5 dB and 3HD ≈ -9 dB. Under small-signal modulation ($m = 0.1$), the photon–photon resonance suppresses the frequency spectrum of chaotic RIN to that of the solitary laser. Examples are given for modulation at $f_m = 9.1$ GHz with $K_{ex} = 0.27$ and $f_m = 9.6$ GHz with $K_{ex} = 0.56$. The reported noise suppression due to the photon–photon resonance is 6 dB stronger than the noise suppression reported in the literature due to the carrier-photon resonance around the relaxation frequency.

This paper was funded by the Deanship of Scientific Research (DSR), King Abdulaziz University, Jeddah, under grant No. 130-057-D1434. The authors, therefore, thankfully acknowledge DSR technical and financial support.

REFERENCES

1. R. W. Tkach and A. R. Chraplyvy, IEEE J. Lightwave Technol. **LT-4**, 1655 (1986).
2. G. P. Agrawal, *Optical Fiber Communication Systems*, Van Nostrand Reinhold, New York (2003).
3. T. Mokai and K. Otsuka, Phys. Rev. **55**, 1711 (1985).
4. K. I. Kallimani and M. J. O'Mahony, IEEE J. Quant. Electron. **34**, 1438 (1998).
5. M. Ahmed and M. Yamada, J. Appl. Phys. **95**, 7573 (2004).
6. M. Yamada, A. Kanamori, and S. Takayama, IEICE Trans. Electron. **E79-C**, 1766 (1996).
7. A. T. Ryan, G. P. Agrawal, G. R. Gray, and E. C. Gage, IEEE J. Quant. Electron. **30**, 668 (1994).
8. J. M. Buldu, F. Rogister, J. Trull et al., J. Opt. B: Quant. Semiclass. Opt. **4**, 415 (2002).
9. K. Stubkjaer and M. B. Small, Electron. Lett. **19**, 388 (1983).
10. E. C. Gage and S. Beckens, Proc. SPIE **1316**, 199 (1990).
11. M. Yamada and T. Higashi, IEEE J. Quant. Electron. **27**, 380 (1991).
12. A. Ohishi, M. Chinone, M. Ojima, and A. Arimoto, Electron. Lett. **2**, 821 (1984).
13. J. Sacher, D. Baums, P. Panknin, W. Elsasser, and E. O. Gobel, Phys. Rev. A **45**, 1893 (1992).
14. M. Yamada, S. Yamamura, and T. Okamoto, IEICE Trans. Electron. **E84-C**, 1588 (2001).
15. G. R. Gray, A. T. Ryan, G. P. Agrawal, and E. C. Gage, Opt. Eng. **32**, 739 (1993).
16. J. C. Yi and H. U. Cho, Phys. Stat. Sol. C **4**, 1617 (2007).
17. M. Ahmed, N. Z. El-Sayed, and H. Ibrahim, Europ. Phys. J. D **66**, 141 (2012).
18. S. M. S. Imran and M. Yamada, IEEE J. Quant. Electron. **49**, 196 (2013).
19. M. Ahmed and M. Yamada, Europ. Phys. J. D **66**, 264 (2012).
20. M. Ahmed, M. Yamada, and S. Abdulrhmann, Int. J. Num. Model. **22**, 434 (2009).
21. Y. H. Kao, N. M. Wang, and H. M. Chen, IEEE J. Quant. Electron. **30**, 1732 (1994).

22. U. Troppenz, J. Kreissl, W. Rehbein, C. Bornholdt, B. Sartorius, and M. Schell, in *Proc. 20th Int. Conf. on Indium Phosphide Related Materials*, Versailles, France (2008), p. 1.

23. H. Dalir and F. Koyama, IEICE Electron. Exp. **8**, 1075 (2011).

24. M. Ahmed, A. Bakry, E. Altuwirqi, M. S. Alghamdi, and F. Koyama, Jpn. J. Appl. Phys. **52**, 124103 (2013).

25. M. Radziunas, A. Glitzky, U. Bandelow et al., IEEE J. Sel. Topics Quant. Electron. **13**, 136 (2007).

26. M. Ahmed, A. Bakry, R. Altuwirqi, M. S. Alghamdi, and F. Koyama, J. Europ. Soc. Opt. Soc. **8**, 13064 (2013).

27. R. Michalzik and K. J. Ebeling, in *Vertical-Cavity Surface-Emitting Laser Devices*, ed. by H. Li and K. Iga, Springer-Verlag, Berlin (2003), ch. 3.

28. M. Ahmed, Physics D **176**, 212 (2003).

29. M. Ahmed, Opt. Laser Technol. **41**, 53 (2009).

30. S. Abdulrhmann, M. Ahmed, and M. Yamada, Proc. SPIE **4986**, 490 (2003).

31. M. Ahmed, M. Yamada, and M. Saito, IEEE J. Quant. Electron. **37**, 1600 (2001).

32. M. Ahmed and A. El-Lafi, Pramana J. Phys. **71**, 99 (2008).

33. M. Ito and T. Kmura, IEEE J. Quant. Electron. **QE-17**, 787 (1981).

34. G. S. Pandian and S. Dilwali, IEEE Photon. Technol. Lett. **4**, 130 (1992).